Stabilization of the elliptical spiral phase and the spin-flop transition in multiferroic $Mn_{1-x}Co_xWO_4$

Y.-S. Song,[1] J.-H. Chung,[1,*] J. M. S. Park,[2] and Y.-N. Choi[2]
[1]*Department of Physics, Korea University, Seoul 136-713, Korea*
[2]*Neutron Science Division, Korea Atomic Energy Research Institute, Daejeon 305-353, Korea*
(Received 3 April 2009; revised manuscript received 27 April 2009; published 12 June 2009)

We have studied the effect of Co doping on the magnetic properties of multiferroic $Mn_{1-x}Co_xWO_4$ using vibrating sample magnetometry and neutron powder diffraction. We find that Co doping at $x \gtrsim 0.05$ suppresses the commensurate AF1 phase and stabilizes the incommensurate spiral AF2 phase down to the lowest temperature. As the Co doping concentration increases further, a spin-flop transition occurs with the spiral-basal plane tilting off the *b* axis. Such magnetic structure expects a ferroelectric polarization component along the *a* axis. The resulting phase diagram is richer than the case of Fe doping.

DOI: 10.1103/PhysRevB.79.224415 PACS number(s): 75.50.Ee, 75.25.+z, 75.30.Kz

I. INTRODUCTION

Coupling between magnetic and electronic degrees of freedom has been attracting a lot of attention in recent years. The magnetoelectric multiferroicity, where ferroelectric polarization develops via exchanges between ordered spins, is one of the most intensively studied among such couplings.[1] These interesting and potentially useful phenomena are observed in a wide class of antiferromagnetic materials possessing long-wavelength spin structures, such as $TbMnO_3$,[2,3] $DyMnO_3$,[3] $TbMn_2O_5$,[4] $CoCr_2O_4$,[5] $Ni_3V_2O_8$,[6] $LuFeO_4$,[7] and $CuFeO_2$.[8] Many of the above listed materials show more than one magnetic phases through successive magnetic transitions. Nevertheless, the magnetoelectric coupling is observed only from particular magnetic phases that feature noncollinear and symmetry-broken spin structures.[9,10] The origin of the magnetoelectric couplings observed in such magnetic structures has been explained by the inverse Dzyaloshinskii-Moriya mechanism, where the ferroelectric polarization is induced by the spin-orbit coupling.[11] In this mechanism, the ferroelectric polarization vector between two spins separated by $\mathbf{e}_{ij}$ is determined as $\mathbf{P}=a\mathbf{e}_{ij}\times(\mathbf{S}_i\times\mathbf{S}_j)$.[12]

The strong correlation between the ferroelectric polarization and the long-wavelength magnetic structure is often evidenced by magnetic field control of the ferroelectric polarization. $MnWO_4$ is one of those materials showing such behavior.[13] It is an antiferromagnet with three different magnetic phases at low temperatures.[14,15] The first antiferromagnetic transition occurs at 13.5 K, where a sinusoidal incommensurate magnetic structure [AF3, $\mathbf{k}_3=(-0.214,\frac{1}{2},0.457)$] is observed.[15] As the temperature is further lowered, it soon changes into a tilted elliptical spiral structure (AF2, $\mathbf{k}_2=\mathbf{k}_3$) at 12.3 K while maintaining the same ordering wave vector,[15] followed by a transition to a collinear commensurate structure [AF1, $\mathbf{k}_1=(\pm\frac{1}{4},\frac{1}{2},\frac{1}{2})$] at 8.0 K.[15] Its ferroelectric polarization is observed along the *b* axis only in the AF2 phase that involves the noncollinear spin arrangement.[13] When the magnetic field is applied along the *b* axis, the temperature range for the AF2 phase is reduced and finally the ferroelectric polarization vector flips to along the *a* axis.[13,16] When the magnetic field is applied perpendicular to the *b* axis, in contrast, the incommensurate AF2 is stabilized down to the base temperature.[16,17] This behavior well demonstrates the strong correlation between the spiral magnetic order and the ferroelectric polarization in $MnWO_4$.

Competitions between different magnetic phases can also be observed when the internal magnetization density is changed via chemical doping. It has been reported that replacement of Mn^{2+} with Fe^{2+} ions stabilizes the commensurate order. As a result, the temperature range for the magnetoelectric AF2 phase becomes narrower up to $x \approx 0.12$, beyond which it is replaced by a simple collinear antiferromagnetic phase [AF4, $\mathbf{k}_4=(\frac{1}{2},0,0)$].[18] Interestingly, the AF2 phase reappears beyond $x \approx 0.22$, and coexists with the AF4.[18,19] Such behaviors suggest that the magnetic phases of $MnWO_4$ are established out of competitions and subtle balance among complicated multiple magnetic interactions.

In this paper, we report the effect of Co doping on the magnetic properties and the phase evolution of the multiferroic $MnWO_4$. The phase diagram obtained by magnetic-susceptibility measurements and neutron powder diffraction is shown in Fig. 1 for the convenience of the readers. The main result of this study is that the Co doping at low con-

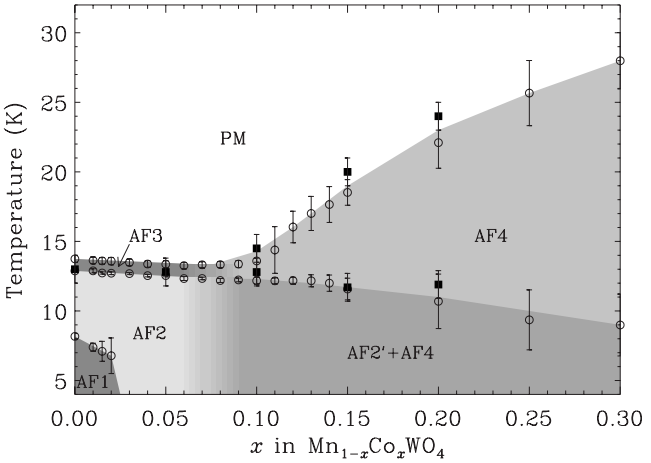

FIG. 1. *x-T* phase diagram of $Mn_{1-x}Co_xWO_4$. The empty circles are obtained from midpoints of the steps that are observed in $d\chi/dT$. The filled squares are onsets of net magnetization obtained from neutron diffraction, which are shown in Fig. 7(c).

centrations shows a contrasting behavior with respect to Fe doping, and stabilizes the incommensurate elliptical spiral AF2 phase at the expense of the commensurate AF1 phase. At high doping concentrations, the magnetic anisotropy is changed leading to a flop of the spiral-basal plane.

II. EXPERIMENTAL

Powder samples of $Mn_{1-x}Co_xWO_4(0.0 \leq x \leq 0.3)$ were synthesized using standard solid-state reactions. High-purity reagents were thoroughly mixed and annealed at 950 °C for 20 h with intermediate grindings. The synthesized samples were confirmed to be single phases by x-ray diffraction. dc magnetic susceptibility was measured with the vibrating sample magnetometry using Quantum Design's Physical Property Measurement System. Applied magnetic field was 1000 Oe for all measurements.

Neutron-diffraction measurements on selected powder samples were performed using High Resolution Powder Diffractometer at HANARO Center of the Korea Atomic Energy Research Institute. A Ge(331) monochromator was used to produce a monochromatic neutron beam at the wavelength of 1.8345 Å. Powder samples were sealed in He-filled vanadium containers and cooled down using a closed-cycle refrigerator. The diffraction intensity was then collected by 32 He-3 proportional counters. The structure analysis was performed using the Rietveld refinement facility of the FULLPROF program.[20]

III. RESULTS AND DISCUSSIONS

A. Magnetic susceptibility

Figures 2(a) and 2(b) show the temperature dependence of the magnetic susceptibility and its inverse, respectively, of selected $Mn_{1-x}Co_xWO_4$ powder samples. The paramagnetic (PM) signal does not change very much when Co doping is introduced at low concentrations, and it is noticeably reduced only for concentrations higher than $x=0.20$. A similar behavior is also noticeable from the inverse susceptibility. Nevertheless, all the magnetic anomalies are observed below 30 K. Close-up views of the susceptibility curves below 30 K are shown in Fig. 2(c). The undoped $MnWO_4$ shows a typical antiferromagnetic anomaly at 13.5 K indicating the onset of the incommensurate sinusoidal AF3 phase, followed by a small downturn at 12.3 K due to a subsequent transition to the spiral AF2 phase. Finally a sharp downturn is observed at 7.8 K, indicating a transition into the commensurate AF1 phase. Interestingly, we notice that this AF2/AF1 phase boundary shifts to lower temperature as soon as the Co dopant is introduced. As the concentration is further increased, the transition becomes diffusive instead of further lowering of the transition temperature. The inset in Fig. 2(c) shows that the corresponding peak in $d\chi/dT$ becomes broader and weaker, and finally almost invisible at $x=0.03$. This result indicates that the Co^{2+} doping favors and stabilizes the AF2 phase that shows magnetoelectric coupling. This behavior is in a clear contrast with the effect of Fe doping, by which the temperature range for the stable AF2 phase is slightly reduced.[18]

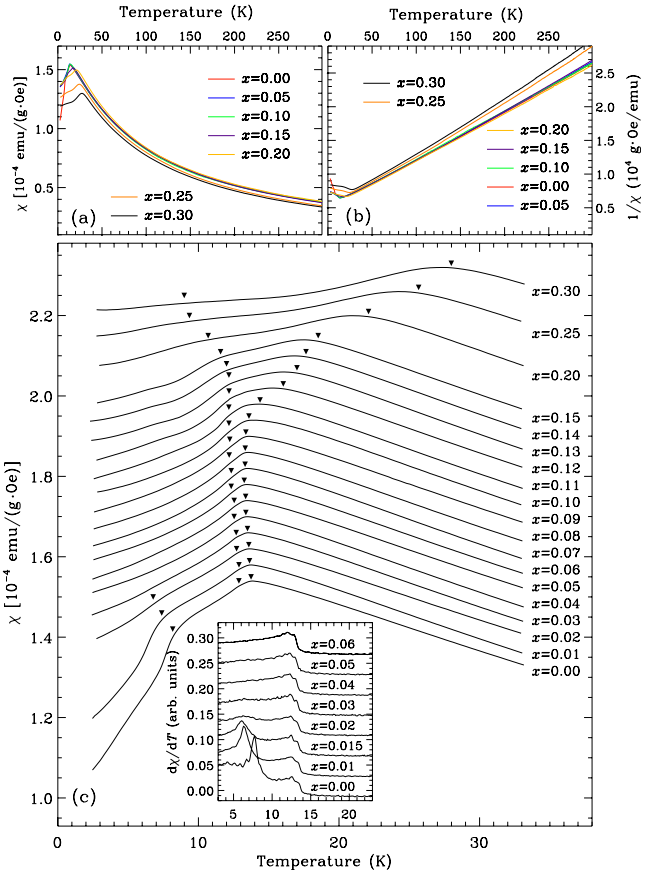

FIG. 2. (Color online) (a) Magnetic susceptibility and (b) inverse susceptibility of $Mn_{1-x}Co_xWO_4$ measured at $B=1000$ Oe. Low temperature part of the magnetic susceptibility curves, shifted vertically for clarity, is shown in (c). The downward triangles indicate transition temperatures obtained from $d\chi/dT$ curves shown in the inset.

On the other hand, the PM/AF3 or the AF3/AF2 boundaries are nearly independent of doping concentration up to $x \gtrsim 0.1$. The existence of the two transitions within a narrow temperature range is better noticed as double steps in the $d\chi/dT$ curves shown in the inset of Fig. 2(c). It is apparent that this feature is nearly invariant over the range of $0 \leq x \leq 0.1$. We note that the corresponding phase boundaries gradually shift to higher temperature in the case of Fe doping.[18] For $x>0.1$, the susceptibility curves show two clear anomalies, the upper one moving up to higher temperature as a function of Co concentration while the lower one moving to the opposite direction. This behavior at high concentration is fairly similar to the case of Fe doping.

We have estimated the magnetic transition temperatures for each sample from the positions corresponding to the half height of the steps observed in the $d\chi/dT$ curve. The obtained temperatures are indicated as downward triangles in Fig. 2(c), and later will be used to map out the x-T phase diagram of $Mn_{1-x}Co_xWO_4$. While we may have an overall idea of the x-T phase diagram based on these results, it is necessary to identify each phase using a direct probe to observe associated magnetic order. The relevant results are discussed in the next section.

TABLE I. Basis vectors for the irreducible representations for axial mode at the Mn sites in space-group $P2/c$ for the propagation-vector $\mathbf{k}=(k_x,\frac{1}{2},k_z)$ ($\psi=e^{-\pi i k_z}$).

Position	$(1/2,y,1/4)$	$(1/2,-y,3/4)$
τ_1^1	(1,0,0)	$(\psi,0,0)$
τ_1^2	(0,1,0)	$(0,-\psi,0)$
τ_1^3	(0,0,1)	$(0,0,\psi)$
τ_2^1	(1,0,0)	$(-\psi,0,0)$
τ_2^2	(0,1,0)	$(0,\psi,0)$
τ_2^3	(0,0,1)	$(0,0,-\psi)$

B. Magnetic structure analysis

In order to identify the nature of each magnetic phase, we performed neutron powder diffraction on selected compositions and analyzed their spin structures using the Rietveld refinement.[20] Starting models for the spin-structure analysis are adopted from the previous report by Lautenschläger *et al.*[15] The basis functions for the irreducible representations for Mn^{2+} spins in $MnWO_4$ are calculated for the propagation-vector $\mathbf{k}=(k_x,\frac{1}{2},k_z)$ from the group theory and summarized in Table I. We note that the same set of basis vectors shown in Table I can be applied to all of the magnetic phases discussed in this paper except for the AF4. For instance, one can obtain basis vectors for the commensurate AF1 phase by taking $k_z=1/2$. In order to generate elliptical spiral with uniform pitches along the c axis, one should use a set of basis vectors from either $(\tau_1^1,\tau_2^2,\tau_1^3)$ or $(\tau_2^1,\tau_1^2,\tau_2^3)$. These two different sets of basis vectors produce spiral chains with opposite chirality from each other, which cannot be discriminated by unpolarized neutron scattering.

Figure 3 shows the observed and the calculated neutron powder diffraction intensities of $MnWO_4$ in the three different phases: (a) PM, (b) AF2, and (c) AF1. Rietveld refinement confirms that the AF1 phase at 4 K has a collinear magnetic structure with the commensurate propagation-vector $\mathbf{k}_1=(-\frac{1}{4},\frac{1}{2},\frac{1}{2})$, and the AF2 phase at 9 K has an elliptical spiral structure with the incommensurate propagation-vector $\mathbf{k}_2=(-0.214,\frac{1}{2},0.457)$. The basal plane of the spiral includes b axis and form an angle of 39° with the a axis. The magnetic Bragg peaks of $MnWO_4$ observed at low-scattering angle are highlighted in Fig. 4(a). The presence of the incommensurate AF2 phase is easily recognized by the double peak observed at $2\theta\approx 15°$. Finally at 13 K and above, magnetic Bragg peaks almost disappear and are replaced by a broad distribution of diffusive intensity due to remanent short-range magnetic interactions. We did not attempt to identify the high-temperature AF3 phase using neutron powder diffraction, because its magnetic Bragg peaks are very weak while the propagation vector is equal to that of the AF2.

In contrast, $Mn_{0.95}Co_{0.05}WO_4$ does not show the commensurate AF1 phase at 4 K. Figure 4(b) indicates that the incommensurate peaks indeed persist down to the lowest observed temperature, where the neutron-diffraction intensity can be well reproduced using the single incommensurate magnetic phase. It is consistent with the temperature dependence of the magnetic susceptibility, which shows no anomaly below 12 K. From the Rietveld refinement, we find that the propagation vector is slightly enlarged to $\mathbf{k}_2=(-0.216,\frac{1}{2},0.461)$, and the angle between the a axis and the spiral-basal plane is reduced to 20°.

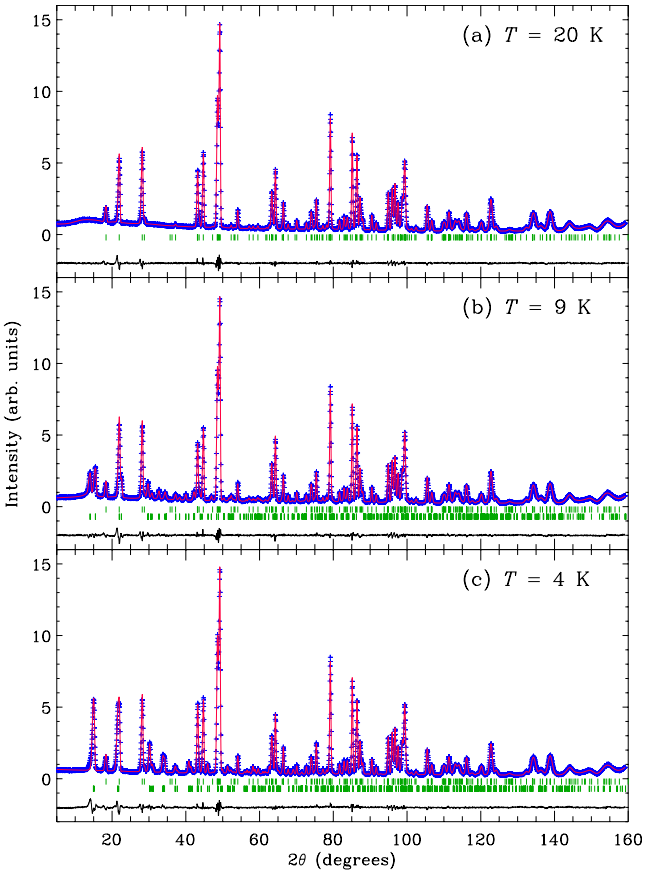

FIG. 3. (Color online) Neutron powder diffraction profiles of $MnWO_4$ at (a) paramagnetic, (b) AF2, and (c) AF1 phases, respectively. The blue crosses and the red lines overlapped indicate experimental and calculated intensities, respectively. The solid line at the bottom of each figure is the difference between the two intensities. The vertical marks indicate Bragg-peak positions of the nuclear (upper row) and the magnetic (lower row) phases.

When the Co concentration is increased to $x=0.1$, the incommensurate peaks are still observed at 4 K with further increased propagation vector [see Figs. 4(c) and 4(d)]. We notice, however, there are two significant changes. First, we notice that there is an additional intensity at ≈11°, which slightly enhances above 10 K and disappears beyond 14 K. It belongs to the commensurate propagation vector at $\mathbf{k}_4=(\frac{1}{2},0,0)$ for $CoWO_4$.[21] We will refer to this phase as AF4 in the rest of the paper. Second, while the peaks are observed at the same locations as the AF2 phase, the intensities of certain peaks are not well reproduced using the same elliptical spiral model. Figure 5(b) shows that the agreement is poor between the experimental and the calculated magnetic Bragg-peak intensities observed in the range of $2\theta=29\sim35°$.

In the AF2 phase, the orientation of the spin vector at $\mathbf{r}=(x,y,z)$ can be expressed as

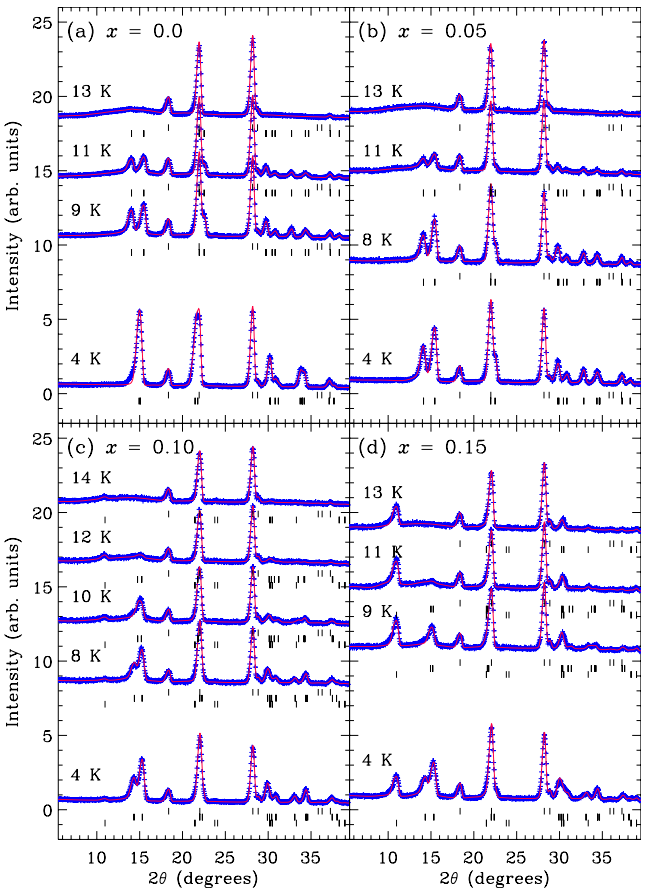

FIG. 4. (Color online) Experimental and calculated neutron powder diffraction intensities of $Mn_{1-x}Co_xWO_4$ observed at low angle revealing magnetic Bragg peaks. (a) $x=0.0$, (b) $x=0.05$, (c) $x=0.10$, and (d) $x=0.15$.

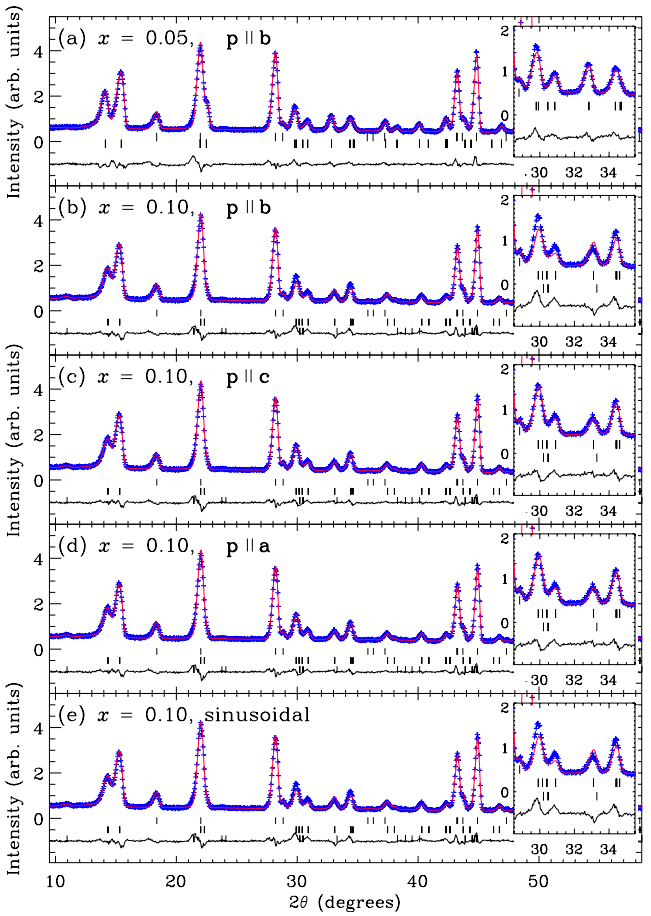

FIG. 5. (Color online) Experimental and calculated magnetic neutron powder diffraction intensities and their differences of (a) $Mn_{0.95}Co_{0.05}WO_4$ and (b)–(e) $Mn_{0.9}Co_{0.1}WO_4$ at 4 K. The calculated profiles are based on elliptical spirals with (a,b) $\mathbf{p}\|\mathbf{b}$, (c) $\mathbf{p}\|\mathbf{c}$, and (d) $\mathbf{p}\|\mathbf{a}$, respectively. The calculation shown in (e) is based on the sinusoidal model.

$$\mathbf{m}(\mathbf{r}) = \mathbf{p}\cos(2\pi\mathbf{k}_2\cdot\mathbf{r}+\phi) + \mathbf{q}\sin(2\pi\mathbf{k}_2\cdot\mathbf{r}+\phi). \quad (1)$$

Above, $\mathbf{p}$ and $\mathbf{q}$ are perpendicular to each other, and the spiral becomes elliptical when $|\mathbf{p}|\neq|\mathbf{q}|$. For $x\leq 0.05$, $\mathbf{p}$ is parallel to the b axis and $\mathbf{q}$ lies in the ac plane.[15] Figure 5(a) shows that the magnetic Bragg peaks observed for $x=0.05$ are reasonably well reproduced using this spin structure. In contrast, Fig. 5(b) shows that the same model fails to reproduce the observed intensity for $x=0.10$. The peaks showing the largest discrepancy are highlighted in the insets of Fig. 5. We find that good agreements are recovered when $\mathbf{p}$ is parallel to either the c or the a axes. As shown in Figs. 5(c) and 5(d), these two models equally well reproduce the observed intensity and our data cannot discriminate between the two. Nevertheless, it clearly indicates that the basal plane of the elliptical spiral tilts off the b axis. We will refer to this phase as AF2′. Figure 5(e) also confirms that we can rule out the sinusoidal model of the AF3 phase.

The spin structures obtained from the Rietveld refinement are summarized in Fig. 6. The AF1 and the AF2 structures for the undoped, shown in Figs. 6(a) and 6(b), respectively, are essentially identical to the previous results.[13,15] In comparison, the spiral-basal plane of $Mn_{0.95}Co_{0.05}WO_4$ is lying closer to the ab plane, resulting in substantial reduction in the c component [see Fig. 6(c)]. Since the ferroelectric polarization is determined by $\mathbf{P}=a\mathbf{e}_{ij}\times(\mathbf{S}_i\times\mathbf{S}_j)$,[12,22] the magnitude of the ferroelectric polarization will probably become smaller in $Mn_{0.95}Co_{0.05}WO_4$. It is also suggested, however, that large ferroelectric polarization will be regained for $x\geq 0.1$. The magnitude of the $\mathbf{P}$ vector in the elliptical spiral phases can approximately be written as

$$P = ae\frac{m_x^2+m_y^2+m_z^2}{2}\sin\pi k_z\sin\delta, \quad (2)$$

where (m_x,m_y,m_z) are the Fourier components of the magnetic moments, and δ is the angle between the c axis and the vector normal to the spiral plane. In the AF2 of the undoped, we find $\sin\delta=m_z/\sqrt{m_x^2+m_z^2}=0.63$, which decreases for smaller m_z at $x=0.05$. In contrast, the two possible AF2′ structures commonly show small m_y, that is $m_y\approx 0.2\sqrt{m_x^2+m_z^2}$. Since it is $\sin\delta\geq 0.96$ in either structure, we expect that the AF2′ phase will possess large ferroelectric polarization primarily along the a axis.

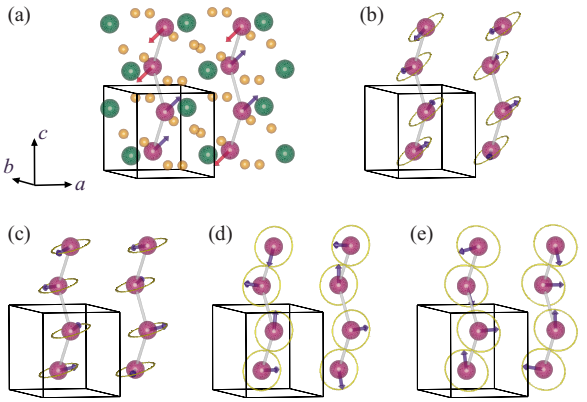

FIG. 6. (Color online) Spin structures of $Mn_{1-x}Co_xWO_4$ obtained from Rietveld refinement of neutron powder diffraction data. (a) $MnWO_4$ at 4 (AF1), (b) at 9 (AF2), and (c) $Mn_{0.95}Co_{0.05}WO_4$ at 4 K (AF2). Shown in (d) and (e) are two possible structures of $Mn_{0.9}Co_{0.1}WO_4$ at 4 K (AF2′), where the spiral plane includes c or a axis, respectively. In (b)–(e), only the Mn/Co sites are drawn for simplicity.

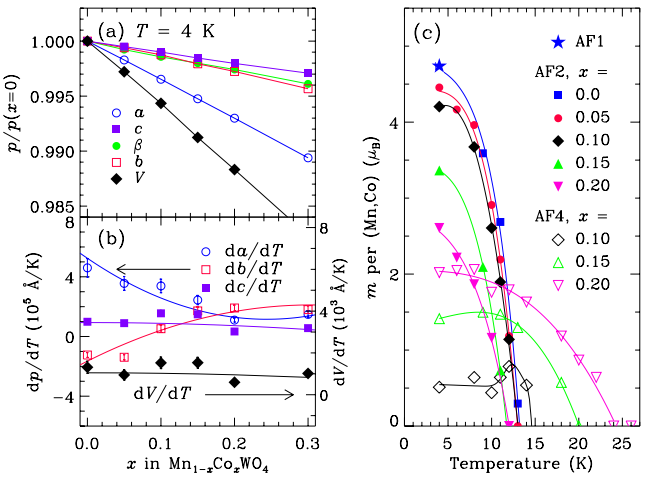

FIG. 7. (Color online) (a) Doping dependence of various structural parameters at 4 K and (b) their temperature coefficients. (c) Temperature dependence of net magnetization per (Mn,Co) site.

C. Phase diagram

By combining the results of the temperature-dependent magnetic susceptibility and neutron powder diffraction, we map out the x-T phase diagram of $Mn_{1-x}Co_xWO_4$ and show it in Fig. 1. The empty circles are obtained by locating the temperatures where steplike anomalies in the $d\chi/dT$ curves reach half of their heights. On the other hand, the filled squares are obtained independently from the onsets of the net magnetization observed in the neutron powder diffraction data. The gaps between the two symbols are ascribed to the different methods employed to estimate the transition temperatures. Those obtained from neutron diffraction are typically higher because they indicate the onsets of magnetic-order parameter. The gaps apparently become larger at higher concentrations where broad and diffusive transitions are observed from the magnetic susceptibility.

The overall phase diagram at a glance may look similar to the case of Fe doping, showing a strong tendency to be dominated by the AF4 phase at high concentrations.[18] Also observed is a coexistence between the AF2′ and the AF4 phases at low temperatures, which is reminiscent of the coexistence between the AF2 and the AF4 in $Mn_{1-x}Fe_xWO_4$. The behaviors at low concentrations, however, are significantly different between the two dopants. Apparently, Fe doping gradually stabilizes the commensurate AF1 phase and shifts the AF1/AF2 phase boundary to higher temperatures.[18] In contrast, the AF1 phase quickly disappears as soon as Co doping is introduced at $x \lesssim 0.05$. As the Co concentration is further increased, the AF2 phase is changed to the AF2′ and coexists with the AF4. We note that the AF2/AF2′ phases are continuously observed over the doping range studied. It is contrasted with the two discontinuous ranges of the AF2 phase observed in $Mn_{1-x}Fe_xWO_4$.[18] Since magnetic susceptibility did not show any noticeable anomaly that can be associated with this spin flop, we suppose the corresponding transition occurs gradually.

We have summarized in Fig. 7 some of the important crystal parameters obtained from the Rietveld refinement. A closer look at the magnetic-order parameters insinuates that the coexistence between the AF2′ and the AF4 phases is not due to compositional inhomogeneity, but is indeed intrinsic to $Mn_{1-x}Co_xWO_4$. Figure 7(c) shows that the order parameter for the AF4 of $Mn_{0.9}Co_{0.1}WO_4$ slightly enhances around 11 K just below the PM/AF4 phase boundary. The enhancement of the corresponding magnetic Bragg peak is also noticeable from the neutron powder diffraction intensity shown in Fig. 4(c). We note that this temperature coincides with the range where the AF2′ phase rapidly melts away. This behavior, also observed for $x=0.15$, indicates a competition between the two magnetic phases that are incompatible with each other. Such competition has previously been noticed in $Mn_{0.88}Fe_{0.12}WO_4$,[19] and seems to be a generic property of doped $MnWO_4$. It is probably ascribable to the subtle balance of complex magnetic interactions in the monoclinic lattice, in which broad distributions of bond distances and angles are observed.

Given the fact that both $Fe^{2+}(3d^6)$ and $Co^{2+}(3d^7)$ ions have smaller magnetic moments than $Mn^{2+}(3d^5)$, the contrasting behaviors of the two dopants may be counterintuitive. Similarly to the previously discussed phase competition, we suspect that it is also due to the marginal magnetic property of $MnWO_4$. We note that $MnWO_4$ is the only antiferromagnetic material showing multiple magnetic transitions among the tungsten wolframites. Its magnetic property even involves high degree of geometrical frustration, which is evidenced by the fairly large ratio between its Curie-Weiss temperature and Néel temperature ($-\Theta_{CW}/T_{N,1}=5.2$). Recently, a similar elliptical spiral phase has been proposed to exist in $Ba_3Mn_2O_8$, whose origin was explained by the combination of geometrical frustration and single-ion anisotropy.[23] In this material, the triangular symmetry of the lattice is responsible for the geometrical frustration. The case of $MnWO_4$ must be even more complicated due to its monoclinic symmetry. A quantitative study using neutron spectroscopy reported that

one requires as many as nine exchange parameters to reproduce its spin-wave excitation spectra, and also single-ion anisotropies accounting for the spin gap.[24] Therefore, it poses a bigger challenge in understanding the magnetic transitions of $MnWO_4$.

We suspect that its complex magnetism and transitions are closely tied to the temperature-dependent changes in the lattice. Figure 7(a) shows that the lattice parameters as well as the unit-cell volume linearly decrease with Co doping, reflecting the smaller radii of Co^{2+} ions. The temperature coefficients of the lattice parameters, however, show interesting behaviors. Figure 7(b) shows that the undoped $MnWO_4$ has a large positive coefficient for a but a negative coefficient for b. As the temperature is increased, the temperature coefficients with opposite signs will affect the balance between the interchain and the intrachain magnetic interactions. Apparently, Co doping at $x > 0.1$ settles positive values of all three parameters as well as the unit-cell volume. Therefore, it seems that lattice instability is responsible for the complex magnetic-phase transitions of $MnWO_4$ involving the incommensurate elliptical spiral phase.

IV. SUMMARY AND CONCLUSION

In summary, we have studied the phase diagram of multiferroic $Mn_{1-x}Co_xWO_4$ using vibrating sample magnetometry and neutron powder diffraction. At low doping concentrations, the incommensurate elliptical spiral AF2 phase is quickly stabilized at the expense of the commensurate AF1 phase. As the concentration is increased to $x \geq 0.1$, the spiral-basal plane tilts off the b axis and coexists with the AF4 phase. We could not, however, discriminate between the two possible AF2′ structures from the analysis of the powder-diffraction intensity. Further work using single-crystal samples will be able to resolve this issue.

ACKNOWLEDGMENTS

We are grateful for helpful discussions with K. H. Kim and L. Yan. This work was supported by the Korea Science and Engineering Foundation (KOSEF) grants funded by the Korean government (MEST) (Grant No. 20090059529), the Nuclear R&D Programs (Grant No. M20701050003-08N0105-00311), and also through the BAERI Program.

*jaehc@korea.ac.kr

[1] S.-W. Cheong and M. Mostovoy, Nature Mater. **6**, 13 (2007).
[2] T. Kimura, T. Goto, H. Shintani, T. Arima, and Y. Tokura, Nature (London) **426**, 55 (2003).
[3] T. Goto, T. Kimura, G. Lawes, A. P. Ramirez, and Y. Tokura, Phys. Rev. Lett. **92**, 257201 (2004).
[4] N. Hur, S. Park, P. A. Shama, J. S. Ahn, S. Guha, and S.-W. Cheong, Nature (London) **429**, 392 (2004).
[5] Y. Yamasaki, S. Miyasaka, Y. Kaneko, J.-P. He, T. Arima, and Y. Tokura, Phys. Rev. Lett. **96**, 207204 (2006).
[6] G. Lawes, A. B. Harris, T. Kimura, N. Rogado, R. J. Cava, A. Aharony, O. Entin-Wohlman, T. Yildrim, M. Kenzelmann, C. Broholm, and A. P. Ramirez, Phys. Rev. Lett. **95**, 087205 (2005).
[7] N. Ikeda, H. Ohsumi, K. Ohwada, K. Ishii, T. Inami, K. Kakurai, Y. Murakami, K. Yoshii, S. Mori, Y. Horibe, and H. Kito, Nature (London) **436**, 1136 (2005).
[8] T. Kimura, J. C. Lashley, and A. P. Ramirez, Phys. Rev. B **73**, 220401(R) (2006).
[9] M. Kenzelmann, A. B. Harris, S. Jonas, C. Broholm, J. Schefer, S. B. Kim, C. L. Zhang, S.-W. Cheong, O. P. Vajk, and J. W. Lynn, Phys. Rev. Lett. **95**, 087206 (2005).
[10] L. C. Chapon, P. G. Radaelli, G. R. Blake, S. Park, and S.-W. Cheong, Phys. Rev. Lett. **96**, 097601 (2006).
[11] H. Sagayama, K. Taniguchi, N. Abe, T. Arima, M. Soda, M. Matsuura, and K. Hirota, Phys. Rev. B **77**, 220407(R) (2008).
[12] H. Katsura, N. Nagaosa, and A. V. Balatsky, Phys. Rev. Lett. **95**, 057205 (2005).
[13] K. Taniguchi, N. Abe, T. Takenobu, Y. Iwasa, and T. Arima, Phys. Rev. Lett. **97**, 097203 (2006).
[14] H. Dachs, H. Weitzel, and E. Stoll, Solid State Commun. **4**, 473 (1966).
[15] G. Lautenschläger, H. Weitzel, T. Vogt, R. Hock, A. Böhm, M. Bonnet, and H. Fuess, Phys. Rev. B **48**, 6087 (1993).
[16] A. H. Arkenbout, T. T. M. Palstra, T. Siegrist, and T. Kimura, Phys. Rev. B **74**, 184431 (2006).
[17] K. Taniguchi, N. Abe, H. Sagayama, S. Otani, T. Takenobu, Y. Iwasa, and T. Arima, Phys. Rev. B **77**, 064408 (2008).
[18] E. García-Matres, N. Stüßer, M. Hofmann, and M. Reehuis, Eur. Phys. J. B **32**, 35 (2003).
[19] N. Stüßer, Y. Ding, M. Hofmann, M. Reehuis, B. Ouladdiaf, G. Ehlers, D. Günther, M. Meißner, and M. Steiner, J. Phys.: Condens. Matter **13**, 2753 (2001).
[20] J. Rodríguez-Carvajal, Physica B **192**, 55 (1993).
[21] J. B. Forsyth and C. Wilkinson, J. Phys.: Condens. Matter **6**, 3073 (1994).
[22] I. A. Sergienko and E. Dagotto, Phys. Rev. B **73**, 094434 (2006).
[23] E. C. Samulon, Y.-J. Jo, P. Sengupta, C. D. Batista, M. Jaime, L. Balicas, and I. R. Fisher, Phys. Rev. B **77**, 214441 (2008).
[24] H. Ehrenberg, H. Weitzel, H. Fuess, and B. Hennion, J. Phys.: Condens. Matter **11**, 2649 (1999).